Journal of Materials Chemistry A

Accepted Manuscript

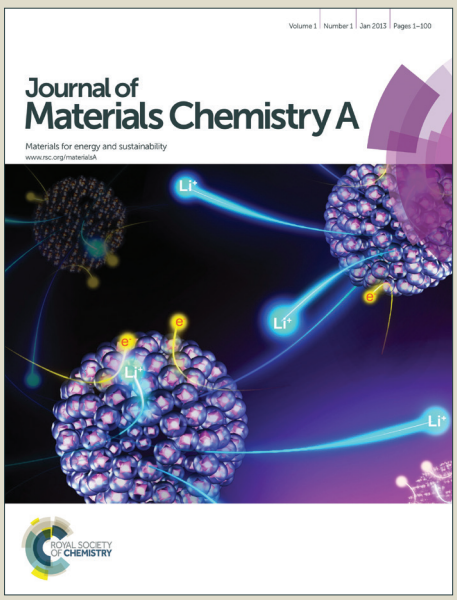

ROYAL SOCIETY OF CHEMISTRY

www.rsc.org/materialsA

Journal Name

RSCPublishing

ARTICLE

Effect of Bulk and Surface Structural Changes in Li_5FeO_4 Positive Electrodes during First Charging on Subsequent Lithium-Ion Battery Performance †

Toyoki Okumura,* Masahiro Shikano, Hironori Kobayashi*

Cite this: DOI: 10.1039/x0xx00000x

Received 00th January 2012,
Accepted 00th January 2012

DOI: 10.1039/x0xx00000x

www.rsc.org/

Bulk and surface structural changes induced in a Li_5FeO_4 positive electrode with a defect anti-fluorite type structure are examined during its initial charge/discharge cycle by various synchrotron-radiation analysis techniques, with a view to determining the contribution of oxygen to its electrochemical properties. Bulk structural analyses including XRD, Fe *K*-edge XANES and EXAFS reveal that pseudo-cubic lithium iron oxides (PC-LFO), in the form of $Li_\alpha Fe^{(4-\alpha)+}O_2$, are formed during the first charging process instead of the decomposition of pristine Li_5FeO_4. Moreover, the relative volume of this PC-LFO phase varies nonlinear according to the charging depth. At the same time, the surface lithium compounds such as Li_2O cover over the PC-LFO phase, which also contribute to the overall electrochemical reaction, as measured from the O *K*-edge XANES operated in a surface-sensitive total-electron yield mode. The ratio of these two different reaction mechanisms changes with the depth during the first charging process, with this tendency causing variation in the subsequent discharge capacity retention in relation to the depth of the charging electron and/or temperature of this "Li-rich" positive electrode. Indeed, such behaviour is noted to be very similar to the specific electrochemical properties of Li_2MnO_3.

1. Introduction

The present scope of application of lithium-ion batteries (LIBs) has expanded well beyond their initial use in small consumer devices such as laptops and mobile phones to incorporate much larger transportation and stationery uses, such as electric vehicles.[1,2] As such, the development of more advanced positive electrode materials, capable of delivering large quantities of Li^+ ions, is essential to the development of LIBs with a higher energy density that are required by these newly emerging applications.[3]

Layered rock-salt $LiCoO_2$ and doped $LiCo_{1-x}M_xO_2$ (*M* = Ni, Mn, Al etc.) structures are currently the most commonly used options for the positive electrodes of most commercial LIBs, due to their relatively high reversible capacity (*ca.* 150 mAh g^{-1}) and cyclability when the cell voltage is controlled within *ca.* 0.5 mol of intercalated/de-intercalated Li^+ ions per layered oxide.[4,5] However, any further increase in Li^+ ion extraction invariably results in degradation of the LIB if it is not suitably modified, such as by application of a surface coating. Moreover, the charged $Li_{1-x}CoO_2$ is not stable under elevated temperatures, whilst the relative rarity and toxicity of cobalt presents a high cost and environmental burden.

Recently, a "Li-rich" layered rock-salt positive electrode based on Li_2MnO_3 has been suggested as a possible alternative[6-9] on the basis that after an initial charging process 4.5 V vs. Li/Li^+, a high reversible capacity of up to 200 mAh g^{-1} can be obtained by the preparation of solid solutions with layered $LiMO_2$ (*M* = Co, Ni, Mn etc.)[6-8,10] or nano-sized particles,[11] or by rendering it oxygen deficient.[12] Many researchers have focused on the unique irreversible reaction that occurs during the first charging process, in addition to the traditional Li^+ ion de-intercalation mechanism, as understanding the overall mechanism would expand the possibilities for advanced positive electrodes in LIBs. Of the several mechanisms proposed thus far, there is a common origin in the preferential removal of electrons from O 2*p* orbitals hybridized with metal orbitals and/or the removal of oxygen atom accompanied by lithium extraction.[6-10,12] This is sometimes rephrased more simply as the removal of Li_2O from the Li_2MnO_3 ($MnO_2 + Li_2O$) component.[6] The other mechanism proposed is a surface reaction of oxygen molecules and/or Li^+/H^+ exchange.[7,13]

Herein, we have chosen to concentrate on the defect anti-fluorite type structure of Li_5FeO_4 as a potential advanced positive electrode material for two main reasons: Firstly, the low-cost, abundance and relative safety of iron-based compounds means they are quite likely to be readily accepted for commercial use. Indeed, many researchers have previously investigated the electrochemical properties of various crystalline-forms of $LiFeO_2$, which has included an α-form, layered, goethite-type, hollandite-type, and a corrugated layered structures.[14-21] Although the preparation of nano-sized particles is necessary to extract an optimal electrochemical

activity, due largely to their inherently low electrical conductivity and lack of Li^+ ion diffusion pathways, especially in disordered α-, β-, and γ-$LiFeO_2$, the development of environmentally-friendly iron-based positive electrodes is vital.[22] Secondly, Li_5FeO_4 ($LiFeO_2$ + $2Li_2O$) can be regarded as belonging to the "Li-rich" electrode family.[23] Until now, a specific reaction mechanism that incorporates the contribution of oxygen has only been reported in the case of Li-rich "layered" oxide Li_2MnO_3, as mentioned above. An understanding as to the structural changes during the first charging cycle on the subsequent reversible capacity of "Li-rich" anti-fluorite structured Li_5FeO_4 is therefore essential to a comprehensive understanding of the specific reaction in advanced "Li-rich" positive electrodes.

The defect anti-fluorite type structure of Li_5FeO_4 is defined by a Fe^{3+} ion substituting for three Li^+ ions in a 2 × 2 × 2 Li_2O cubic *Fm*-3*m* primitive cell, thereby creating a crystallographic orthorhombic symmetry (space group of *Pbca*).[23,24] Both the Li^+ and Fe^{3+} ions (and vacancy) occupy 8*c* tetrahedral sites in a close-packed array of O^{2-} ions, whilst a $Fe^{3+}O_4$ tetrahedron is isolated by adjacent Li^+O_4 tetrahedra and vacancies. A high first charging capacity of over 694 mAh g^{-1} can be obtained when four Li^+ ions (or two Li_2O) are removed from the Li_5FeO_4 unit cell,[23] although the subsequent reversible capacity could not observed because the isolated FeO_4 tetrahedra are decomposed by the drastic removal of Li^+ ions. In 2003, Imanishi *et al.* reported that the subsequent reversible capacity could be observed by controlling the Li^+ ion removal process of the first charging (x = 1.0 – 2.0 in $Li_{5-x}FeO_4$), in which the reversibility is changed by the value of x.[25-27] This first-charging profile, and the change in reversibility by x, for Li_5FeO_4 is similar to recently reported values for Li_2MnO_3 and related compounds.[11] By measuring the valence change of iron ions by Mössbauer spectroscopy during the charge-discharge process, it has been found that the Li^+ ion removal process during the first charging cannot be explained without at least some contribution by oxygen.[26] Furthermore, Johnson *et al.* have reported the oxidation of iron ions at x = 2 on the basis of Fe *K*-edge X-ray absorption near-edge structure (XANES) spectra, as well as by Li_2O removal in chemically de-lithiated samples.[23]

In the present paper, the bulk structural change induced in an advanced Li_5FeO_4 positive electrode during its first charging is systematically investigated by Rietveld refinements of synchrotron X-ray diffraction (XRD) profiles and Fe *K*-edge X-ray absorption fine structure (XAFS) spectra, including both XANES and extended X-ray absorption fine structure (EXAFS). This change in surface structure is subsequently discussed in relation to O *K*-edge XANES spectra obtained by a surface-sensitive total-electron yield mode, which is intended to shed new light on the specific electrochemical reaction of this "Li-rich" positive electrode. Differences in the subsequent reversibility in relation to the depth of Li^+ ion removal during the first charging process are also discussed.

2. Experimental Procedure

Li_5FeO_4 was synthesized via a solid-state reaction, in which $LiOH{\cdot}H_2O$ (99.0%, Kishida Chemical Co.) and $FeC_6H_5O_7{\cdot}nH_2O$ (Wako Pure Chemical Industries) were used as the starting materials. The required amount of each starting material was first mixed in a platinum crucible, and then added to 5 ml of distilled water. The resulting slurry was heated to 800 °C for 12 h under an Ar flow, and then cold-pressed into pellets in an Ar filled grove box and re-heated under the same conditions. A laboratory XRD pattern of the synthesized product was collected on a RINT-TTR diffractometer using Cu Kα radiation, whilst the morphology was analysed by field-emission scanning electron microscopy (FE-SEM, JEOL, JSM-5500LV).

Synchrotron XRD and XAFS analyses of the pristine and electrochemically reacted Li_5FeO_4 samples were carried out to investigate the charge-discharge profiles. The electrode consisted of a suspension containing 60 wt% active material, 32 wt% acetylene black (AB), and 8 wt% polytetrafluoroethylene (PTFE) that was mixed and pressed, and then hollowed out to a size of ϕ9 by a round punch. The electrodes were assembled in a two-electrode cell using metallic lithium foil as a counter/reference electrode and a liquid electrode of 1 mol dm^{-3} of $LiPF_6$ in an ethylene carbonate/dimethyl carbonate solution. The electrochemical charge-discharge profiles were all obtained at a constant current of 1/30 C. XRD analysis was used to examine the crystalline phases present in each sample at a wavelength of 0.5 Å, and was conducted at BL19B2, SPring-8, Sayo, Japan (2012B1598). Rietveld crystal structure refinements of the XRD patterns obtained were performed using the RIETAN-FP program.[28] For this, we selected a pseudo-Voigt function for the fitting method, in order to best represent the profile parameters of the samples. Hard X-ray absorption fine structure (XAFS) spectroscopy was conducted at BL12C, Photon Factory, Tsukuba, Japan (2012G707), and at BL14B2, SPring-8, Sayo, Japan (2013B1810), using the Fe *K*-edge to investigate both the electronic and local structures of pristine and electrochemically charged/discharged samples, which were subsequently analysed by XANES and EXAFS, respectively. All spectra were recorded in transmission mode. Fourier transformations were performed for k^3-weighted EXAFS oscillations using Rigaku REX2000 data analysis software.[29] Finally, soft XANES spectroscopy was conducted at BL4B, UVSOR, Okazaki, Japan, using the O *K*-edge to investigate the surface electronic structure. All measurements were recorded in a surface-sensitive total-electron yield mode.

3. Results and Discussion

The signature peaks observed in the laboratory XRD pattern of the synthesized product all correspond to a simulated pattern for a low temperature phase of Li_5FeO_4 (space group of *Pbca*).[24] Meanwhile, SEM imaging indicated that the Li_5FeO_4 powder used was composed of 20–50 μm sized particles. Both this XRD pattern and SEM image of Li_5FeO_4 are summarized in ESI, Figs. S1 and S2, respectively.†

Fig. 1 shows the electrochemical charge-discharge profiles of Li_5FeO_4 obtained at 25 and 50 °C, in which approximately two electrons per Li_5FeO_4 contribute to the electrochemical reaction during the first charging process (the specific capacity is *ca.* 347 mAh g^{-1}). This produces a long plateau during the first charging cycle that is observable around 3.5 V *vs.* Li/Li^+,

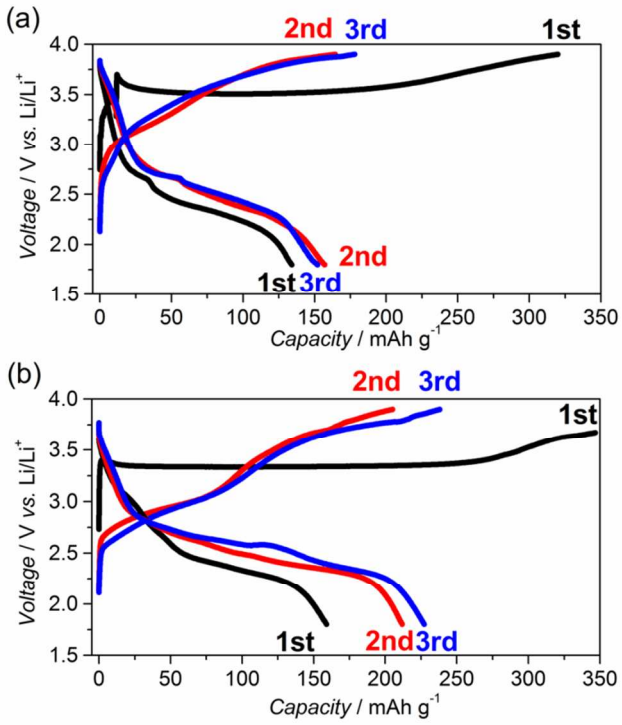

Fig. 1 Electrochemical charge-discharge profiles for a Li_5FeO_4 positive electrode, as determined by a galvanostatic method operated at (a) 25 °C and (b) 50 °C (C rate: 1/30 C, capacity limit: cut-off voltage of 1.7–3.9 V *vs.* Li/Li^+ or until two electrons react per Li_5FeO_4). Note that a small current of 1/300 C was applied for 10 h to prevent a rapid potential increase at the beginning of the first charging at (a) 25 °C.

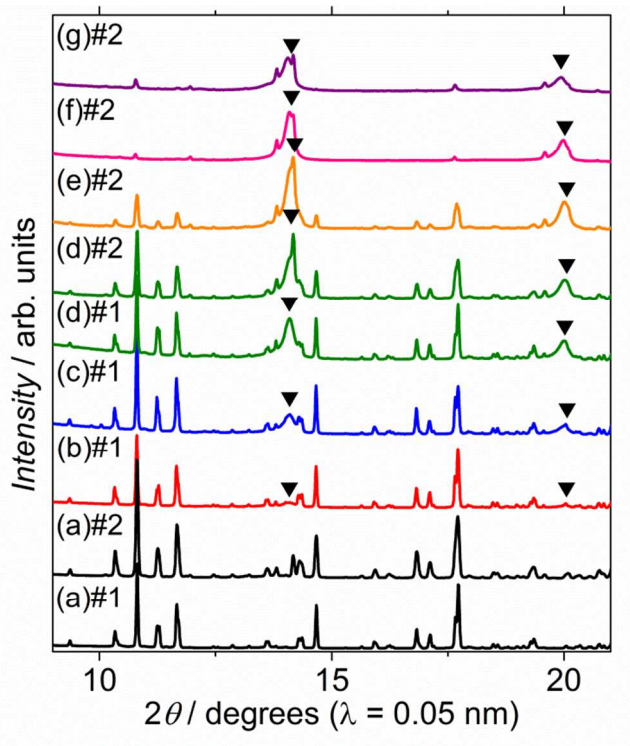

Fig. 2 *Ex situ* synchrotron X-ray diffraction patterns of electrochemical samples halted during the first charging process. The number of charged electrons per positive electrode is (a) $e = 0$ (pristine), (b) 0.33 (charged until 58 mAh g^{-1}), (c) 0.66 (charged until 116 mAh g^{-1}), (d) 1 (charged until 173 mAh g^{-1}), (e) 1.5 (charged until 260 mAh g^{-1}) and (f) 1.85 (fully charged until 320 mAh g^{-1}). (g) *Ex situ* synchrotron X-ray diffraction patterns of a fully discharged sample (discharged until 134 mAh g^{-1}). The differences between the two batches of #1 and #2 are also shown. The patterns associated with the $Li_\alpha FeO_2$ (PC-LFO) phase are represented by black triangles.

as has been reported previously.[23,25-27] Furthermore, the duration of this voltage plateau increases with temperature, which is a result of the suppression of inner-cell resistances. The reversible capacities were observed during subsequent charge-discharge cycles, but these exhibited a very different profile to that of the first charging process. This suggests that the characteristics of the subsequent charge-discharge cycles are influenced by the electrochemical reaction of products from the first charging process, which is confirmed by the structural analyses discussed in section 3.1 of this study. Similar characteristics are also evident in Li_2MnO_3, which also exhibits a long plateau during the first charging process and subsequent charge-discharge cycles.[11]

3.1. Structural change during the first charge/discharge cycle

3.1.1. Rietveld analysis of synchrotron XRD data

Synchrotron XRD profiles from obtained for samples subjected to varying degrees of electrochemical reaction so as clearly visualize the phase changes during charging or discharging, as shown in Fig. 2. From this, it is evident that although the synthesized powder was sintered several times prior to fabricating the batteries, tiny impurities such as α-$LiFeO_2$ and Fe metal are very difficult to remove effectively. It should also be noted that two separate sets of synchrotron XRD data were obtained, with the amount of impurities differing between them. Nevertheless, these impurities are considered irrelevant to the present discussion, since they were all found to electrochemically inactive within the measured potential range. More important is the observation that the peaks corresponding to the synthesized Li_5FeO_4 phase all decrease with charging (oxidized) depth, whilst at the same time, additional broad peaks appear around 14 and 20° during charging that are associated with small grains of a pseudo-cubic $Li_\alpha FeO_2$ (PC-LFO) reaction product. Imanishi *et al.* have already suggested the possibility of a cubic α-$LiFeO_2$ phase from laboratory XRD results, and noted that not all of the peaks coincided.[26] In present paper, Rietveld refinements were performed in order to determine this phase change in more detail.

Fig. 3 (a) shows the result of Rietveld refinement of the synchrotron XRD pattern of a pristine positive electrode. These refinements were applied in the range of 9–40°, since the appearance of halo patterns for AB at around 7.5° and the peaks of PTFE at 5.4° make the refinement more complicated. Most of the visible pattern is well fitted to an orthorhombic phase (space group of *Pbca*), which suggests a low temperature phase of Li_5FeO_4 in conjunction with lesser patterns attributable to the trace amounts of impurities. The results of *ex situ* electrochemically charged and discharged samples are also shown in Fig. 3 (b) and (c), respectively. From this, it is clear that the profile of the PC-LFO phase at its fully charged state fits well with the simulated pattern of a FeO_2 cubic phase (space

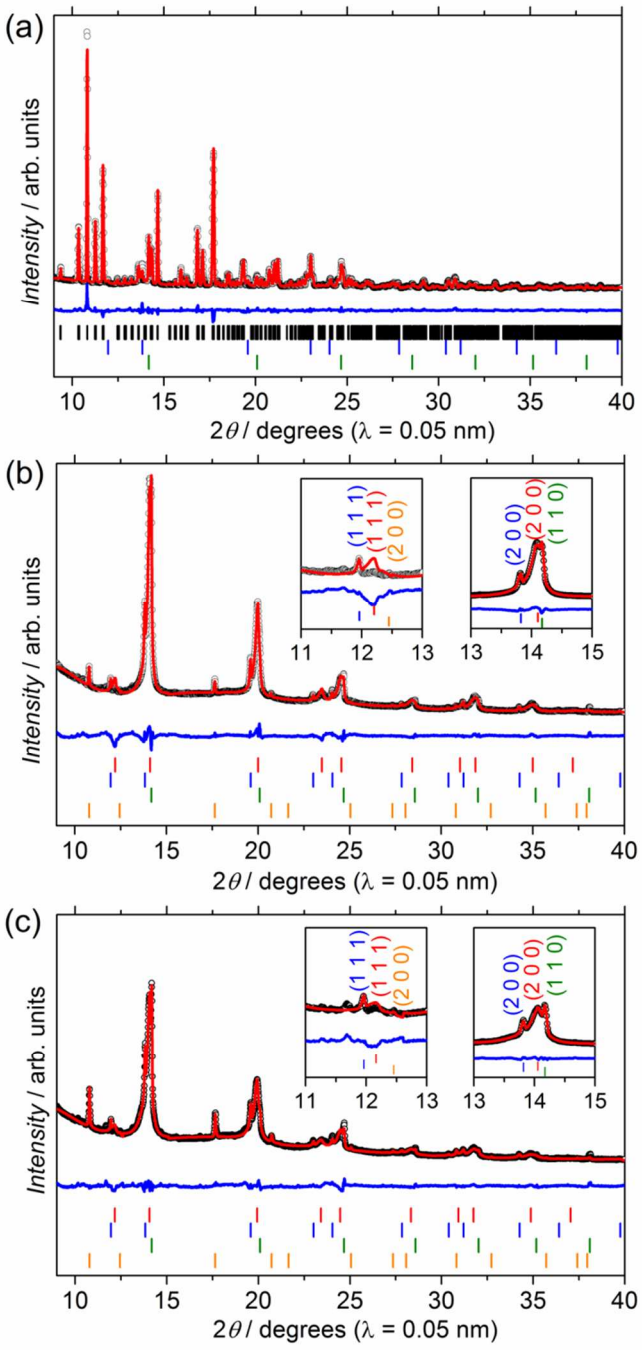

Fig. 3 Rietveld refinements of *ex situ* synchrotron X-ray diffraction patterns of (a) pristine, (b) fully charged until 320 mAh g^{-1} (e = 1.85) and (c) fully discharged until 134 mAh g^{-1} (e = 0.77) samples. The observed, calculated and difference plots are shown by black open circles, red solid lines, and blue solid lines, respectively. Diffraction positions are indicated by several colour bars: black (Li_5FeO_4), red (generated PC-LFO; $Li_\alpha FeO_2$), blue ($LiFeO_2$ impurity), green (Fe impurity), and orange (Li_2O).

group of *Fm*-3*m*); a notable exception is the intensity of *I*(111) at around 12.2°, which is shown more clearly in the inset of Fig. 3 (b). The simulated FeO_2 phase possesses a cubic rock-salt structure, which is similar to the structure of α-$LiFeO_2$. (A lattice parameter *a* of α-$LiFeO_2$ is 4.162 Å.)[30] Since the lattice parameter *a* (= 4.073 Å)

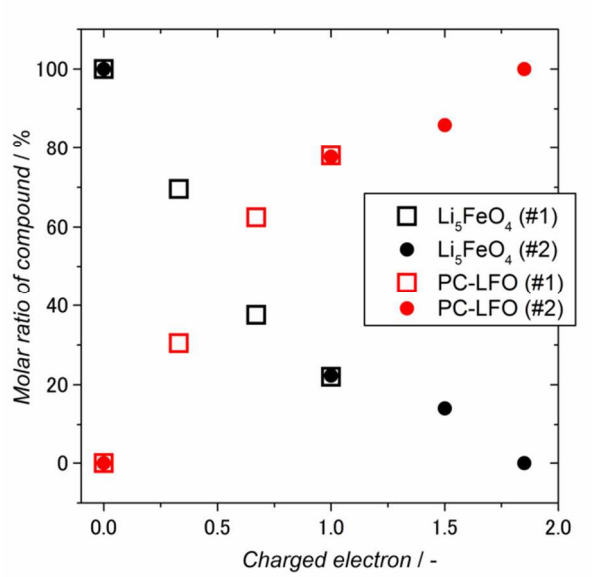

Fig. 4 Molar ratios of Li_5FeO_4 and PC-LFO ($Li_\alpha FeO_2$), as estimated by Rietveld refinement of synchrotron X-ray diffraction patterns.

of the PC-LFO phase was smaller than that of reported α-$LiFeO_2$, the valence of iron ion in PC-LFO ($Li_\alpha Fe^{(4-\alpha)+}O_2$) would be close to 4+ (based on ionic radii of Fe^{3+} and Fe^{4+} of 0.645 and 0.585 Å, respectively.)[31] The mismatch of *I*(111) between the observed and simulated profiles can therefore be explained by the lattice distortion of the PC-LFO phase. Note that the Li^+ site was deliberately omitted from this analysis, because the X-ray scattering factor of lithium is far too small to estimate. Refinement of this profile was also attempted by other phases of lower symmetry, such as tetrahedral or hexagonal structures, but a sufficient match could not be obtained. Nonetheless, it is clear that the PC-LFO phase possesses a lower symmetry, and is thus hereafter referred to as a "pseudo-cubic" phase. All of the PC-LFO phases appearing in the *ex* situ electrochemically charged and discharged samples are therefore easily analysed by using a cubic rock-salt FeO_2 structure, as shown in ESI, Fig. S3.†

The molar ratios of Li_5FeO_4 and PC-LFO phases in various charged samples are shown in Fig. 4. From this, it is evident that a PC-LFO phase is actively produced at the very beginning of the charging process due to decomposition of the Li_5FeO_4 phase. Since the production of this PC-LFO phase requires a considerable amount of Li and O to be released from the Li_5FeO_4 phase, it stands to reason that some lithium compounds must also be generated (e.g., Li_2O, Li_2O_2, Li_2CO_3, amorphous phases, etc.), both with and without the evolution of oxygen gas. Thus, not only are small PC-LFO grains produced on the surface of Li_5FeO_4, but also some lithium compounds. Furthermore, since the PC-LFO phase is less produced toward the end of the charge process, it is the other reaction that is predominate in the oxidation of the positive electrode. One possibility for this is that Li^+ ions are removed from the PC-LFO phase already produced; however, this should produce shrinkage of the PC-LFO lattice due to the oxidation of iron, which was not observed in the synchrotron X-ray diffraction profiles. The alternative is that the lithium compounds generated are further

oxidized, and although the oxidation of lithium compounds is difficult to ascertain by X-ray, the Li_2O phase (orange bars) identified in the profile of the fully charged sample (Fig. 3 (b)) provides some proof of the existence of lithium compounds. Moreover, the existence of this Li_2O phase has been previously identified in lithiated $Li_{5+x}FeO_4$.[32] Unfortunately, although SEM-EDX analysis was performed on these positive electrode samples, the lithium compounds in question are unlikely to be of sufficient thickness to be discernible by this method of analysis.

At a fully discharged state, the PC-LFO phase was maintained without any evidence for reformation of the Li_5FeO_4 phase. Furthermore, the expansion of the lattice parameter, α, for the PC-LFO from 4.073 to 4.086 Å indicates a reduction of the PC-LFO phase by the intercalation of Li^+ ion. The mismatch of $I(111)$ estimated from a fully charged sample (Fig. 3 (b)) also suppressed in the fully discharged sample, as shown in inset of Fig. 3 (c). Again, this can be attributed to reduction of the PC-LFO phase, and then a relaxation of the structural distortion with the injection of electrons. It is also worth noting that the amount of Li_2O phase observed in the fully discharged sample (23 mol% of the PC-LFO phase) was much than that in the fully charged sample (10 mol% of the PC-LFO phase). This unique result indicates that the Li_2O generated during the charging process are also subject to electrochemical reactions during discharging.

3.1.2. Fe *K*-edge XANES

The synchrotron Fe *K*-edge XANES spectra of samples electrochemically charged to various stages were measured so as to analyse the electronic structural variations that accompany the phase change from Li_5FeO_4 to PC-LFO phase, and are shown in Fig. 5 (a). The XANES spectra of 3*d* transition metals is described by a combination of parameters: the selection rule, the coordination number, the number of *d*-electrons, and the symmetry of the coordination sphere.[33] For instance, the main peak of A (A_1-A_3 or A_1'-A_2') is simply represented by an electric dipole-transition from the core Fe 1*s* orbital to an unoccupied Fe 4*p* orbital, due to the dipole selection rule. Moreover, the peak in the transition metal *K*-edge XANES spectrum provides information as to the oxidation state of the absorbing atom and the local geometric structure. The shoulder peak B is ascribed as the cause of the dipole-allowed Fe 1*s* orbital to Fe 4*p* orbital transition, thus leading to a final state of $1s1c\ 3d^{n+1}L\ 4p^1$), with a shakedown process that originated from a ligand to metal charge transfer, in which *L* is a ligand hole. The high intensity of this shoulder peak B is readily confirmed in the XANES spectrum of the pristine Li_5FeO_4 phase (black solid line), since the Fe 4*p* orbital strongly overlaps with the O 2*p* (ligand) orbital in a FeO_4 tetrahedral coordination, a phenomenon which can also be seen in γ-$LiAlO_2$: Fe^{3+}.[34] The main peaks of A_1-A_3 and shoulder peak B are also very different to the Fe_2O_3 reference (black dash line), which possesses FeO_6 octahedron due to localised geometric structural differences. However, the energy slope of the main peak for pristine Li_5FeO_4 is very close to that of the Fe_2O_3 reference, indicating that the valence state of iron was 3+. During charging, these main peaks of A_1-A_3 in the pristine FeO_4-tetrahedra-coordinated Li_5FeO_4 sample gradually change to peaks of A_1' and A_2' due to the formation of the

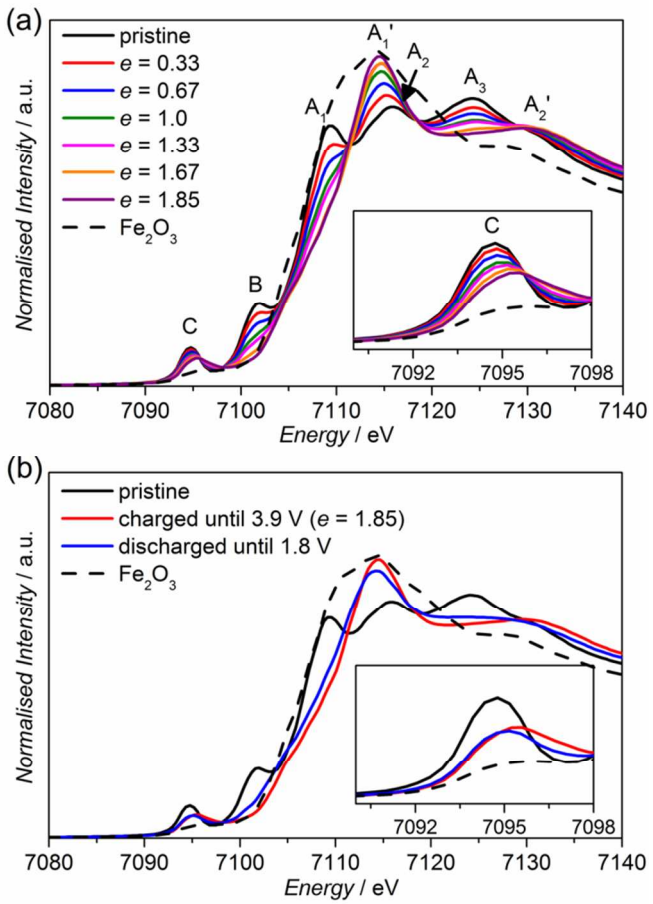

Fig. 5 *Ex situ* Fe *K*-edge XANES spectra of (a) electrochemical samples halted during the first charging process, (b) electrochemically charged/discharged samples.

FeO_6-octahedra-coordinated PC-LFO phase, as confirmed by the synchrotron XRD analysis. The energy slope of main peak for pristine $Li_5Fe^{3+}O_4$ is also shifted to a higher energy in relation to the charging depth, since the valence state of iron in the PC-LFO phase is (4-α)+, which is the same as that reported by Johnson *et al.*[23] The coordination difference between tetrahedral Li_5FeO_4 and octahedral PC-LFO also effects the hybridization of the Fe 4*p* and O 2*p* orbitals, thus weakening the intensity of the shoulder peak B. These changes to peaks A and B predominantly occur at the beginning of the charging process (especially, $0 \le e \le 1.0$), and are therefore clearly related to the change in the Li_5FeO_4 to PC-LFO molar ratio, as estimated by the Rietveld refinement of the synchrotron XRD data. The pre-edge peak, C, typically represents the electric-dipole-forbidden transition of a Fe 1*s* electron to a Fe 3*d* orbital, and thus could not appear as a result of this process. Despite this, various explanations for the appearance of the pre-edge have been proposed on the basis of the 4*p* orbital of the absorbing atom mixing with the 3*d* orbital of the neighbouring atoms, or weak electric quadrupole transitions.[33] As can be seen in the inset of Fig. 5 (a), a pre-edge peak C is clearly discernible in the pristine $Li_5Fe^{3+}O_4$ phase, which is due to the mixture of 3*d* and 4*p* orbitals in the FeO_4 tetrahedral coordination.[33,34] The decrease in this peak in relation to charging depth is due to the overlap of 3*d* and 4*p* orbitals being weakened by the coordination change from a FeO_4 tetrahedron to a FeO_6

octahedron. As such, the pre-edge C peak is not evident in the $Fe^{3+}{}_2O_3$ reference sample, as this has high-symmetry FeO_6 coordination. However, a small pre-edge C peak does still remain after the formation of the PC-LFO phase is complete, which can be attributed to a slight mixing of 3*d* and 4*p* orbitals due to local structural distortions in the FeO_6 octahedron of the PC-LFO phase.

The synchrotron Fe *K*-edge XANES spectrum of a fully discharged sample is shown in Fig. 5 (b) alongside the spectra for pristine and fully charged samples. This demonstrates that the energy slope of the main peak in the fully charged PC-LFO phase is slightly shifted to a lower energy in a fully discharged sample, because the valence state of iron is reduced by the intercalation of Li^+ ions into the PC-LFO phase. Furthermore, the discharge capacity of the synthesized positive electrode of 134 mAh g^{-1} means that an *e* of 0.77 is injected into the positive electrode during discharging. Nevertheless, this shift is too small to fully explain the discharging process from the reduction of iron alone. This shortfall can be explained by one of two reasons: electrons are also injected into the ligand O 2*p* orbital strongly hybridized with the Fe 3*d* orbital in the PC-LFO phase and/or other lithium compounds react. It is this unique latter process that is considered to be the more likely, given the increase in Li_2O at a fully discharging state estimated by the Rietveld analysis of the XRD profiles.

3.1.3. Fe *K*-edge EXAFS

In order to investigate the local structure around the Fe atomic centre in electrochemically charged/discharged samples, Fe *K*-edge EXAFS spectra were evaluated. Fig. 6 (a) shows Fourier transforms (FTs) of the EXAFS oscillations for samples electrochemically charged to various stages, which indicates pseudo-radial structure functions (RSFs) within the local atomic environment surrounding the Fe centres. The FTs of the k^3-weighted Fe *K*-edge EXAFS oscillations for the samples were calculated within k = 2.6 – 15.9 $Å^{-1}$ (this range being chosen so as to minimize noise), and are shown in ESI, Fig. S4.† The RSF of the Fe *K*-edge EXAFS oscillation of pristine Li_5FeO_4 (indicated by the black line in Fig. 6 (a)) shows only one A peak at about 1.5 Å, which corresponds to the four coordinated Fe-O bonds in the FeO_4 tetrahedron. The intensity of peak A decreases with charging depth, as shown in Fig. 6 (a). Other inter-atomic interferences were not visible because the FeO_4 tetrahedron is surrounded by a LiO_4 tetrahedron, in which the scattering factor of lithium is too small. The RSF of oscillation, $\chi(k)$, is generally represented by the equation:

$$\chi(k) = \sum_i \frac{NS_0^2 |f(k,\pi)| \exp(-2\sigma_i^2 k^2) \exp(-2R_i/\lambda_i) \sin[2kR_i + \phi_i(k)]}{kR_i^2} \quad (1)$$

where N is the number of neighbouring atoms, $S_0{}^2$ is the amplitude of $\chi(k)$, R is the atomic distance to the neighbouring atom, σ^2 is the Debye-Waller (DW) factor, λ is the mean free path, and ϕ is the total phase shift.[25] Since the N of Fe-O bonds corresponding to peak A should vary from 4 in Li_5FeO_4 to 6 in PC-LFO during the charging process, the intensity should increase, and yet, this contradicts the observed results. This could be caused by the high symmetry of the FeO_4 tetrahedron, in which the strong covalent character of FeO_4 is surrounded by the Li^+ ions of Li_5FeO_4. Note that the intensity of the peak A corresponding to the 6 Fe-O bonds in PC-LFO is relatively similar to that in other FeO_6 coordinated compounds such as Fe_2O_3 or FeO, which were not shown. The full width at half maximum (FWHM) of peak A also thickens as a result of the phase change during charging, ultimately dividing into two peaks, R = 1.4 and 1.8 Å, in the fully charged sample (e = 1.85, purple line in Fig. 6 (a)), which is most likely the result of lattice distortion in the PC-LFO phase. As well as these changes in peak A, an additional peak B corresponding to the Fe-Fe interaction in PC-LFO appeared at around 2.6 Å. Both this decrease in peak A, and increase in peak B, were observed to occur right from the very beginning of the charge process (especially, $0 \leq e \leq 1.0$), which supports the synchrotron XRD and Fe *K*-edge XANES results.

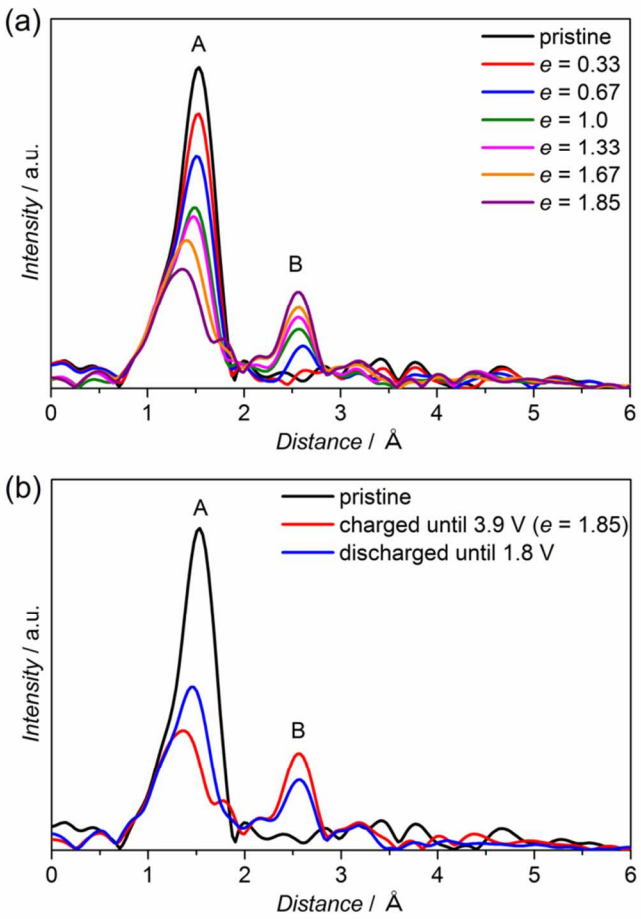

Fig. 6 Fourier transforms of (a) electrochemical samples halted during the first charging process, (b) electrochemically charged/discharged samples, as estimated from *ex situ* Fe *K*-edge EXAFS oscillations.

The FT of the Fe *K*-edge EXAFS oscillation for an electrochemically fully discharged sample is shown in Fig. 6 (b) alongside the oscillations of pristine and fully charged samples. It is evident from this that the FWHM of peak A is made narrower, and the intensity increased, at a fully discharged state, which is due to the relaxation of FeO_6 octahedral distortion. At the same time, the intensity of peak B corresponding to Fe-Fe interaction is reduced. Although the localised structural change during discharging is complicated, it can at least be concluded that the structural change of the PC-LFO phase due to intercalation of Li^+ ions plays some part in the discharging

process. This is also true of the reactions of other lithium compounds on the surface of the PC-LFO phase, which are discussed later in Section 3.1.4 with regards to the O *K*-edge XANES results.

Overall, the structural distortion of the PC-LFO phase was confirmed by the results of XRD, Fe *K*-edge XANES and EXAFS. One possibility is that this is caused by the existence of a Jahn-Teller distorted $Fe^{4+}O_6$ octahedron (the electron configuration of Fe^{4+} ion at high spin state is $t_{2g}^3e_g^1$); however, such discussion is unable to account for the unusually high valence of Fe^{4+} ions in the crystal. For example, with a $SrFeO_3$ perovskite structure, an electron in the e_g orbital of Fe^{4+} ion is delocalized, which means that its electron configuration is $t_{2g}^3e_g^2L$, and its symmetry is cubic.[35] On the other hand, $CaFeO_3$ exhibits charge disproportionation of $2Fe^{4+}$ ($t_{2g}^3e_g^2L$) → Fe^{3+} ($t_{2g}^3e_g^2$) + Fe^{5+} (t_{2g}^3) with a reduction in temperature, and thus its symmetry is distorted to orthorhombic.[36,37] However, this sort of charge disproportionation could not observed in the Fe *K*-edge XANES spectrum of the fully charged PC-LFO phase. Furthermore, the existence of Fe^{5+} was not confirmed by the Mössbauer measurement reported by Imanishi *et al.*[26] Consequently, the structural distortion of the PC-LFO phase could only be caused by a "partial" Jahn-Teller effect of Fe^{4+} ions. Additionally, the injection of electrons into the ligand hole, *L*, in Fe^{4+} ($t_{2g}^3e_g^2L$) was indirectly measured by Fe *K*-edge XANES in the fully discharged PC-LFO phase. Thus, it is clear that the O 2*p* orbital is strongly hybridized with the Fe 3*d* orbital, and therefore exhibits an intermediate electronic behaviour. This hybridized Fe 3*d* - O 2*p* orbital, which is produced by Li_5FeO_4 during the first charging process, also contributes to the overall electrochemical reaction.

3.1.4. O *K*-edge XANES

Fig. 7 shows the O *K*-edge XANES spectra of electrochemically charged/discharged samples measured by a surface-sensitive total-electron yield mode, which demonstrates that the O 2*p* orbital hybridizes with the Fe 3*d*, Fe 4*sp* orbital and Li 2*p* in lithium iron oxides. The absorption peaks in the O *K*-edge XAFS spectra therefore directly reflect the unoccupied O 2*p* orbital connected with coordinated atomic characters.[38] The peaks a and b for Fe_2O_3, which were observed at around 533–538 eV, can be attributed to the transitions of the O 1*s* orbital to the hybridized orbital of O 2*p* with Fe 3*d* t_{2g} and that of O 2*p* with Fe 3*d* e_g in a FeO_6 octahedral coordination, respectively. On the other hand, peak A at around 537 eV results from the LiO_4 tetrahedral coordination of Li_2O. This means that the spectrum of the pristine Li_5FeO_4 sample is closest to that of Li_2O, since the Li_2O possesses the same anti-fluorite type structure. As was found from the structural analysis in the preceding sections, an octahedral FeO_6-coordinated PC-LFO phase is produced during charging. Nevertheless, the characteristic peaks of a and b that are observed in Fe_2O_3 could not be measured, which indicates that the surface of this PC-LFO phase is covered with Li_2O lithium compounds. Since the shape of the spectra around 535–538 eV is changed during charging by the introduction of an additional peak A' at around 536 eV, these Li_2O lithium compounds are clearly involved in the reaction; further, Li_2O_2 is the most likely

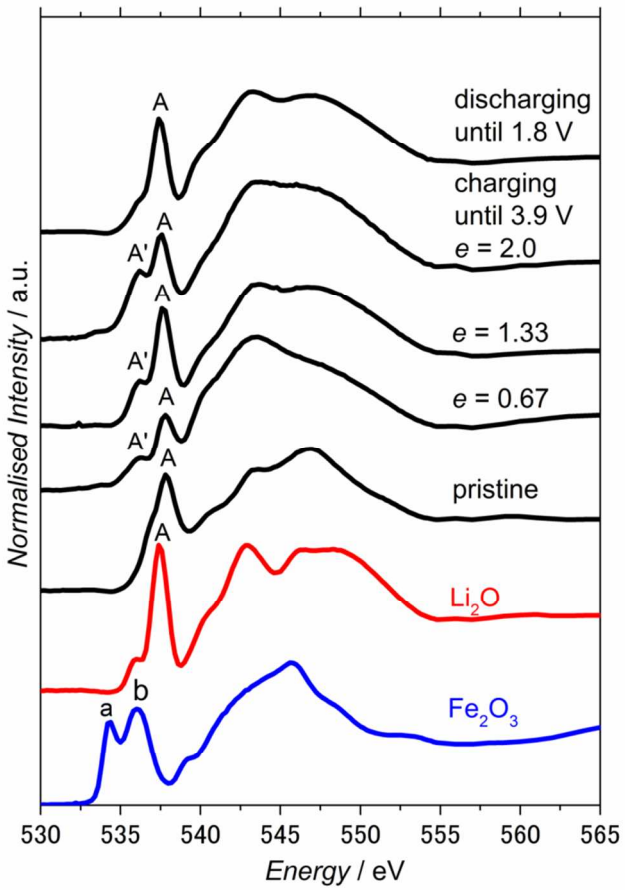

Fig. 7 *Ex situ* O *K*-edge XANES spectra of electrochemically charged/discharged samples, as measured under a total-electron-yield mode.

product to be formed by their oxidation.[39,40] The A' peak was also observed to disappear when Li_2O was re-formed on the surface of the fully discharged PC-LFO sample, and thus, the electrochemical reaction of this surface Li_2O also likely contributes to the electrochemical reaction and structural change of the PC-LFO phase, as evidenced by the de-intercalation of Li^+ ions observed in the Fe *K*-edge XAFS spectra.

3.2. Change in charge/discharge properties with capacity and/or temperature

Fig. 8 shows the electrochemical charge-discharge profiles of Li_5FeO_4 positive electrodes operated for up to 10 cycles at 25 and 50 °C. The charging capacity was controlled to obtain variations of $e \approx 2$ (until 3.9 V), 1.5, and 1; as previously reported,[26] the discharge capacity and profile retention was observed to vary in relation to the depth of the charging electron with each cycle. The operating temperature also had a significant effect of the profiles, with the discharge capacity retention of $e = 1$ at 50 °C proving the best amongst the conditions in this study. It should be noted, however, such an elevation in temperature is likely to cause decomposition of the organic electrode over longer periods of time. The electrochemical reaction at the long plateau observed during the

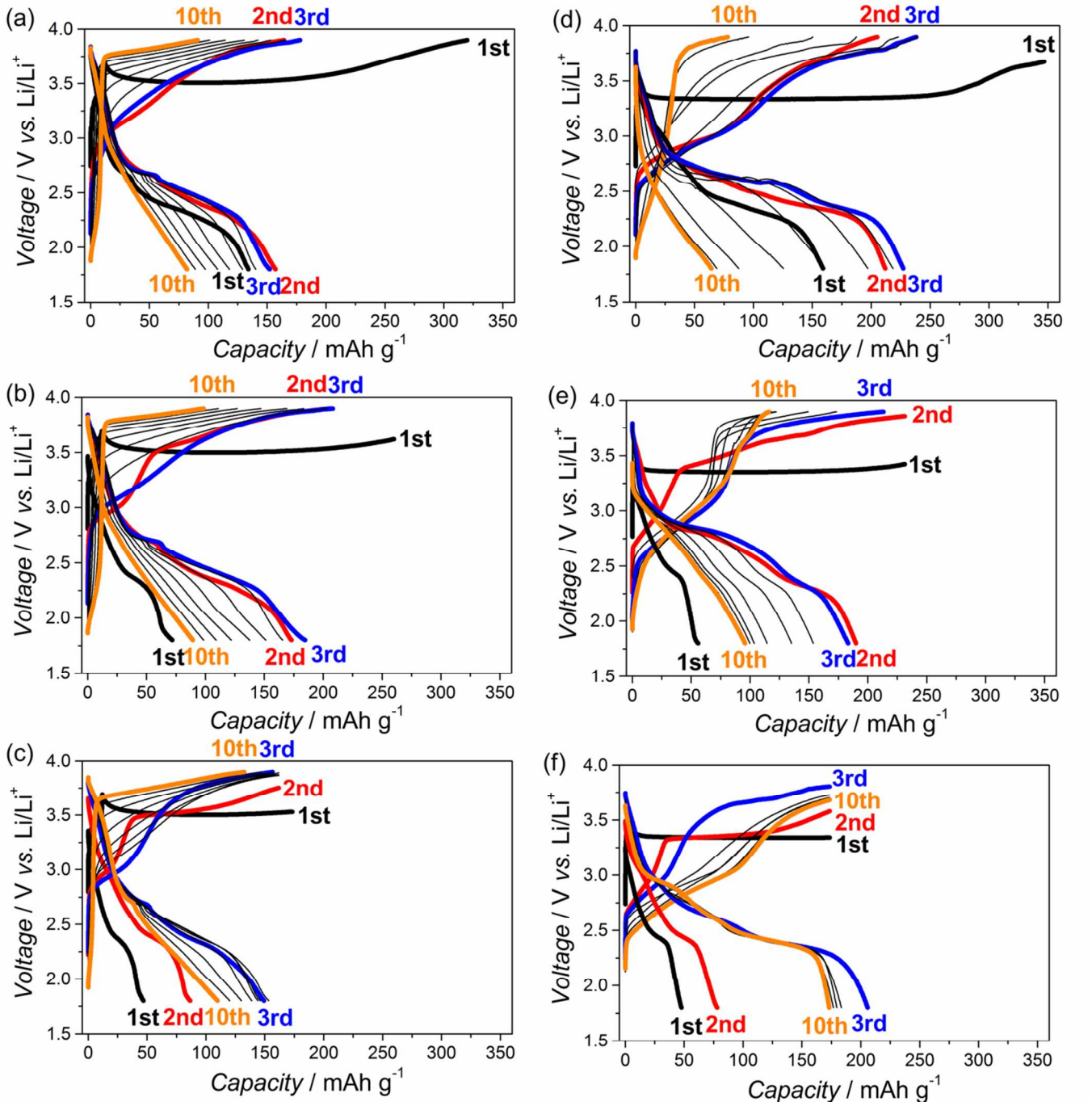

Fig. 8 Electrochemical charge-discharge cycle-performance of Li_5FeO_4 positive electrodes during the first 10 cycles, as determined by galvanostatic testing at (a,b,c) 25 °C and (d,e,f) 50 °C (C rate: 1/30 C, capacity limit: cut-off voltage of 1.7–3.9 V Li/Li^+ or until reacting for (a,d) e = 2, (b,e) e = 1.5, (c,f) e = 1 per Li_5FeO_4). Note that a small current of 1/300 C was applied for 10 h to prevent a rapid potential increase at the beginning of the first charging at (a,b,c) 25 °C.

first charging process can be seen to vary with charging depth, which confirms the earlier structural analysis results. This difference in the discharge capacity retention most likely results from variations in the formation of the PC-LFO phase and/or lithium compounds on the PC-LFO surface, either of which could be readily influenced by the depth of the charging electron and/or temperature.

4. Conclusions

The changes in the crystal and electronic structure of an anti-fluorite type Li_5FeO_4 positive electrode during the first charging and discharging cycle were examined in detail in order to ascertain the specific electrochemical reaction in "Li-rich" positive electrodes. Through synchrotron XRD, Fe *K*-edge XANES and EXAFS analysis, it was found that a pseudo-cubic lithium iron oxide (PC-LFO) phase

of $Li_{\alpha}Fe^{(4-\alpha)+}O_2$ is formed in fully charged samples instead of the decomposition of pristine Li_5FeO_4. The relative ratio of this PC-LFO phase varied nonlinear according to the charging depth, and is therefore likely to a major factor in the observed variation in discharge capacity retention with the depth of charging electron and/or temperature; a similar tendency was observed in the electrochemical properties of Li_2MnO_3.[41]

Structural distortion of the PC-LFO phase in a fully charged state was also estimated from synchrotron XRD, Fe *K*-edge XANES and EXAFS, and attributed to a "partial" Jahn-Teller effect of Fe^{4+} ion. The existence of a ligand hole, *L*, in Fe^{4+} ($t_{2g}^3e_g^2L$) was also indirectly measured by Fe *K*-edge XANES, revealing that the O 2*p* orbital is strongly hybridized with the Fe 3*d* orbital, and therefore contributes to the overall electrochemical reaction. The formation of Li_2O lithium compounds was also detected by synchrotron XRD, with the O *K*-edge XANES spectra of the PC-LFO phase confirming that it was covered with these lithium compounds. Moreover, the electrochemical reaction of this surface Li_2O phase is also believed to contribute to the overall electrochemical reaction.

Thus, the contribution of oxygen to electrochemical behaviour that is well-known in Li_2MnO_3, is considered likely to also occur in advanced "Li-rich" anti-fluorite type Li_5FeO_4 positive electrodes. Presently, the rate capacity and discharge capacity retention of Li_5FeO_4 positive electrodes are quite; however, the results of this study encourage the possibility that a novel "Li-rich" electrode could be designed to offer a far greater discharge capacity.

Acknowledgements

One of the authors (T.O.) is grateful to Dr. H. Ben Yahia for his fruitful discussion regarding Rietveld analysis.

Notes and references

National Institute of Advanced Industrial Science and Technology (AIST), Midorigaoka 1-8-31, Ikeda, Osaka 563-8577, Japan. *E-mail: toyoki-okumura@aist.go.jp; hironori-kobayashi@aist.go.jp

† Electronic supplementary information (ESI) available. See DOI: 10.1039/b000000x/

1 F. T. Wagner, B. Lakshmanan and M. F. Mathias, *J. Phys. Chem. Lett.*, 2010, **1**, 2204.
2 M. Armand and J. -M. Tarascon, *Nature*, 2008, **451**, 652.
3 B. C. Melot and J. -M. Tarascon, *Acc. Chem. Res.*, 2013, **46**, 1226.
4 J. -M. Tarascon and M. Armand, *Nature*, 2001, **414**, 359.
5 J. B. Goodenough and Y. Kim, *Chem. Mater.*, 2010, **22**, 587.
6 M. M. Thackeray, S. –H. Kang, C. S. Johnson, J. T. Vaughey, R. Benedek and S. A. Hackney, *J. Mater. Chem.*, 2007, **17**, 3112.
7 N. Yabuuchi, K. Yoshii, S. -T. Myung, I. Nakai and S. Komaba, *J. Am. Chem. Soc.*, 2011, **133**, 4404.
8 H. Yu and H. Zhou, *J. Phys. Chem. Lett.*, 2013, **4**, 1268.
9 J. Rana, M. Stan, R. Kloepsch, J. Li, G. Schumacher, E. Welter, I. Zizak, J. Banhart and M. Winter, *Adv. Energy Mater.*, 2013, DOI: 10.1002/aenm.201300998.
10 H. Kobayashi, T. Okumura, M. Shikano, K. Takada, Y. Arachi and H. Nitani, *Solid State Ionics*, 2013, http://dx.doi.org/10.1016/j.ssi.2013.09.045.
11 J. Lim, J. Moon, J. Gim, S. Kim, K. Kim, J. Song, J. Kang, W. B. Im and J. Kim, *J. Mater. Chem.*, 2012, **22**, 11772.
12 K. Kubota, T. Kaneko, M. Hirayama, M. Yonemura, Y. Imanari, K. Nakane and R. Kanno, *J. Power Sources*, 2012, **216**, 249.
13 A. R. Armstrong, A. D. Robertson and P. G. Bruce, *J. Power Sources*, 2005, **146**, 275.
14 J. Morales and J. Santos-Peña, *Electrochem. Commun.*, 2007, **9**, 2116.
15 S. -H. Wu and H. -Y. Liu, *J. Power Sources*, 2007, **174**, 789.
16 M. M. Rahman, J. -Z. Wang, M. F. Hassan, S. Chou, Z. Chen and H. K. Liu, *Energy Environ. Sci.*, 2011, **4**, 952.
17 A.E. Abdel-Ghany, A. Mauger, H. Groult, K. Zaghib and C.M. Julien, *J. Power Sources*, 2012, **197**, 285.
18 M. M. Rahman, A. M. Glushenkov, Z. Chen, X. J. Dai, T. Ramireddy and Y. Chen, *Phys. Chem. Chem. Phys.*, 2013, **15**, 20371.
19 Y. Sakurai, H. Arai and J. Yamaki, *Solid State Ionics*, 1998, **29**, 113.
20 A. R. Armstrong, D. W. Tee, F. L. Mantia, P. Novak and P. G. Bruce, *J. Am. Chem. Soc.*, 2008, **130**, 3554.
21 M. Hirayama, H. Tomita, K. Kubota, H. Ido and R. Kanno, *Mater. Res. Bull.*, 2012, **47**, 79.
22 J. Li, J. Li, J. Luo, L. Wang and X. He, *Int. J. Electrochem. Sci.*, 2011, **6**, 1550.
23 C. S. Johnson, S. -H. Kang, J. T. Vaughey, S. V. Pol, M. Balasubramanian and M. M. Tackeray, *Chem. Mater.*, 2010, **22**, 1263.
24 R. Luge and R. Hoppe, *Z. Anorg. Allg. Chem.*, 1984, **513**, 141.
25 S. Narukawa, Y. Takeda, M. Nishijima, N. Imanishi, O. Yamamoto and M. Tabuchi, *Solid State Ionics*, 1999, **122**, 59.
26 A. Hirano, T. Matsumura, M. Ueda, N. Imanishi, Y. Takeda and M. Tabuchi, *Solid State Ionics*, 2005, **176**, 2777.
27 N. Imanishi, Y. Inoue, A. Hirano, M. Ueda, Y. Takeda, H. Sakaebe and M. Tabuchi, *J. Power Sources*, 2005, **146**, 21.
28 F. Izumi and K. Momma, *Solid State Phenom.*, 2007, **130**, 15.
29 J. J. Rehr and R. C. Albers, *Reviews of Modern Physics*, 2000, **72**, 621.
30 M. Vacinic-Vasic, B. Antic, J. Blanusa, S. Radic, A. Kremenovic, A.S. Nikolic and A. Kapor, *Appl. Phys. A: Mater. Sci. Process*, 2006, **82**, 49.
31 R. D. Shannon, *Acta Crystallogr. A*, 1976, **32**, 751.
32 V. A. Maroni, C. S. Johnson, S. C. M. Rood, A. J. Kropf and D. A. Bass, *Appl. Spectroscopy*, 2013, **67**, 903.
33 T. Yamamoto, *X-ray Spectrom.*, 2008, **37**, 572.
34 G. A. Waychunas, M. J. Apted and G. E. Brown Jr., *Phys. Chem. Minerals*, 1983, **10**, 1.
35 P. K. Gallagher, J. B. MacChesney and D. N. E. Buchanan, *J. Chem. Phys.*, 1964, **41**, 2429.
36 M. Takano, N. Nakanishi, Y. Takeda, S. Naka and T. Takada, *Mater. Res. Bull.*, 1977, **12**, 923.
37 T. Mizokawa, *J. Phys: Conf. Ser.*, 2013, **428**, 012020.
38 F. M. F. de Groot, J. Faber, J. J. M. Michiels, M. T. Czyzyk, M. Abbate and J. C. Fuggle, *Phys. Rev. B*, 1993, **48**, 2074.
39 B. M. Gallant, D. G. Kwabi, R. R. Mitchell, J. Zhou, C. V. Thompson and Y. Shao-Horn, *Energy Environ. Soc.*, 2013, **6**, 2518.
40 R. Qiao, Y. –D. Chuang, S. Yan and W. Yang, *Plos One*, 2012, **7**, e49182.
41 A. Ito, D. Li, Y. Ohsawa and Y. Sato, *J. Power Sources*, 2008, **183**, 344.

Table of Contents

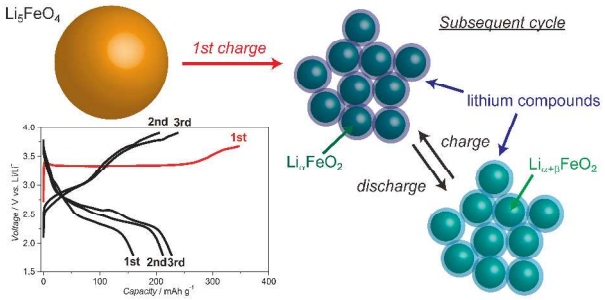

Specific charge/discharge properties of Li_5FeO_4 positive electrodes with regards to bulk and surface structural changes during the first charging process analyzed by synchrotron techniques including XRD, XANES, and EXAFS.